TOWARDS REFINED CONTRAIL SIMULATIONS OF FORMATION FLIGHT SCENARIOS

Judith Pauen, Simon Unterstrasser & Anton Stephan

Institute of Atmospheric Physics, German Aerospace Center (DLR)

Abstract

Flying in formation reduces the climate effect of CO_2 and non-CO_2 emissions from passenger aircraft. In particular, the climate effect of contrail-cirrus can be substantially reduced. A comprehensive understanding of the contrail evolution and spreading is crucial. However, observational data are challenging to obtain, and previous simulations have often relied on idealized initialization settings, even for single-flight scenarios. In this study, we present large-eddy simulation (LES) of the early contrail evolution during the so-called contrail vortex phase, which is characterised by an interplay of ice microphysics and wake vortex dynamics. The objective of this study is to understand the sensitivity of the early contrail evolution to the initialization of the wake vortex flow field. In our previous LES studies, the description of the initial wake vortex flow was based on an analytical Lamb-Oseen vortex profile. In the present studies, the flow initialization is based on a priori Reynolds-Averaged Navier-Stokes simulations (RANS), which model the flow around the complete aircraft geometry, specifically of an A380 and A320.

Our findings indicate that the initialization of the flow field has a substantial impact on the outcome when compared to simulations utilizing previous idealized initialization settings. Notably, not all ice crystals are captured within the RANS-initialized wake vortex system but remain at emission altitude. The analyses presented in this study are a major prerequisite for establishing more realistic contrail simulations behind aircraft formations. In an upcoming study, the contrail LES model will be initialized with a flow field behind a two-aircraft formation that is obtained from a RANS-LES model.

Keywords: CFD, wake vortex dynamics, microphysics, contrail evolution

1. Introduction

In aviation, non-CO_2-effects probably have a larger impact on climate than CO_2-effects [1], with contrail-cirrus having the largest share of the non-CO_2-effects [2]. Therefore, a proper understanding of the characteristics and evolution of contrail-cirrus is fundamental. Observations of long-lived contrails are scarce and difficult to obtain because contrail-cirrus often lose their characteristic linear shape or merge with natural cirrus. Hence, model-based approaches are a promising alternative to obtain more information about their behaviour.

Contrail ice crystals form in the expanding and quickly cooling exhaust plumes of the engine[3]. The formation is completed within one or a few seconds [4, 5]. After the formation phase, the further contrail fate is controlled by the interplay of ice microphysics and the trailing wake vortex system [6, 7]. Much of the initially formed ice crystals are captured by the counter-rotating wake vortex pair and are carried down while the wake vortex pair descends. This results in a vertical expansion of the contrail, yet a significant amount of the entrained ice crystals can get lost due to adiabatic heating. The extent of the contrail varies behind different types of aircraft because, on the one hand, the mass and geometry of the aircraft determine the initial properties of the vortex system and therefore influence the descent of the contrail [8]. On the other hand, the fuel flow regulates the water vapour emission and, in addition to the temperature and fuel properties, also affects the number of ice crystals produced.

Due to detrainment after the vortex break-up, the ice crystals are released from the wake vortex system and rise up due to buoyancy (the upper troposphere is typically stably stratified). After around 10

minutes, direct effects from the aircraft on the contrail evolution have ceased and contrails experience the same microphysical processes that occur in natural cirrus. In an ice-supersaturated environment, ice crystals grow by uptake of water vapour and contrails spread horizontally by vertical wind shear and vertically by sedimentation. Eventually, contrails lose their linear shape and their appearance resembles that of natural cirrus. Hence, persistent contrails are referred to as contrail-cirrus. The properties and the climate relevance of contrail-cirrus depend on many different parameters (relative humidity, temperature, lapse rate, turbulence, vertical shear of crosswind, aircraft geometry/weight, fuel burn, and soot emission index).

Various mitigation options to reduce the climate impact of the contrail-cirrus are under debate. One approach is to re-route flights, such that the aircraft does not fly through ice-supersaturated regions [9], where persistent contrail-cirrus develop. Another approach is to establish formation flight of passenger aircraft. In the military aviation sector, close formation flight with an aircraft separation of a few wing spans is already a standard procedure. In the civil sector, extended formation flight with larger separation distances could be viable. The follower aircraft benefits from the energy of the wake vortex of the leading aircraft. It flies in the upwash region, which leads to a reduction of the induced drag, an increase in lift-to-drag ratio and a lower fuel consumption. In addition, the contrails produced compete for the available atmospheric water vapour, which is required for the growth of the ice crystals. Therefore, the climate impact of the contrail-cirrus from a formation of two aircraft is lower than the summed climate impact of the contrails of two aircraft flying independently from each other [10, 11]. The necessary framework for the operational implementation of formation flight in the current air traffic system and formation flight itself are being investigated in detail by various partners in the SESAR project GEESE.

The influence of aircraft characteristics has already been investigated in several ways: In Paoli et al. [12], an investigation into the entrainment of exhaust jets within the vortex system was conducted, specifically emphasizing disparities observed between two-engine and four-engine aircraft configurations. In a separate study [8], a significant reduction was observed in the ice crystal loss during the vortex phase for a smaller aircraft, e.g. B737, compared to larger aircraft, e.g. B747. Their findings suggested that the vortices from the smaller aircraft, due to a less extensive and slower descent, experienced a reduced ice crystal loss. In-depth in situ measurements of three contrails generated by A319, A340, and A380 aircraft aged around 2 minutes in similar meteorological environments were conducted by JeSSberger et al.[13]. These measurements revealed discernible differences in the microphysical properties among the various aircraft. Specifically, the contrails generated by the A380 exhibited higher ice crystal number concentrations. However, the measurement flights encountered subsaturated conditions, limiting the contrail sampling to very short-lived ones.

The aim of this study is to understand the sensitivity of the early contrail evolution to the initialization of the wake vortex flow field, in particular towards formation flight configurations. Previous EULAG-LCM contrail simulations were initialized with an analytical description of the wake vortex pair, for typical single aircraft scenarios [6] as well as for formation flight configurations [10]. In a first step, we replace this analytical wake vortex initialisation by a more realistic vortex flow field as obtained by a Computational Fluid Dynamics (CFD) near-field simulation of the vortex roll-up process that simulates the velocity field around and behind an aircraft with the codes TAU and TAU-MGLET, both based on the Reynolds-Averaged Navier-Stokes (RANS) equations. It will be analysed whether or how this affects the early contrail evolution for conventional single aircraft case. Moreover, we analyse the contrail evolution for different aircraft types (e.g. A320 and A380). In the present study, we focus on an initialization of the wake vortex phase simulations with data from a detailed RANS simulation of the flow around a complete aircraft. The contrail simulations are carried out for supersaturated scenarios with long-lasting contrails. The contrail evolution is shown first for an A380 and then for the smaller A320 aircraft. For both aircraft types, contrail vortex phase simulations with an analytical wake vortex profile initialization have been presentend in Unterstrasser and Görsch [8] and the new results will be compared to these.

2. Methods

2.1 RANS and RANS-LES models for wake vortex initialization

The CFD simulations of the flow around a fully modelled aircraft are carried out with two different codes, which are used in parallel: On the one hand, the RANS model TAU has been employed and simulation data have been provided by Airbus. On the other hand, we use results from the RANS-LES code TAU-MGLET, which is employed within DLR. Both models are described in the following.

2.1.1 TAU

TAU is a compressible, unstructured, finite volume code that solves the RANS equations [14]. It is a highly accurate, robust, and reliable code that is perfectly suited to resolve the boundary layer and near-field of an aircraft due to its capability to handle complex geometries. For turbulence modeling, a variety of two-equation models and Reynolds stress models are on hand based on the Spalart-Almaras, k-ω and k-ε models. Aiming for robustness and low dissipation, we employ a matrix dissipation scheme, as well as the robust, but accurate Spalart-Almaras model. In time, a second order accurate dual stepping scheme is applied.
TAU has been employed to simulate the flow around the full geometry of an A380 aircraft. For this study, 2D data slices (in planes perpendicular to the flight direction) are available at various downstream positions. We use data for $X = 10\,\mathrm{m}$ and $X = 210\,\mathrm{m}$, where X specifies the distance from the tail of the aircraft to the 2D slice.

2.1.2 TAU-MGLET

MGLET (Multi Grid Large Eddy Turbulence) is an incompressible, finite volume large-eddy simulation (LES) code [15]. It utilizes a dynamic Lagrangian subgrid-scale model and a fourth-order compact finite-volume spatial discretization scheme and the time integration is carried out by an explicit three-step Runge-Kutta scheme. Since compressibility effects are not relevant for the wake-vortex evolution in the atmosphere, the use of an incompressible solver in the far-field is justified [16].
The communication between both codes is done using a coupling module that is part of the development release of TAU in version 2017.1 and explained in Spiering [17].
The Code TAU-MGLET fully couples the two codes described above: TAU (see previous subsection) and MGLET. MGLET solves the flow on a Cartesian background mesh whereas TAU solves the flow directly around the aircraft in a unstructured mesh. The latter domain is moving through the background domain, creating a spatial CFD simulation. Details can be found in Stephan et al. [16].
To simulate the flow around a A320 with full geometry, TAU-MGLET has been utilized. Again, 2D data slices (in planes perpendicular to the flight direction) are available at the downstream positions $X = 4.3\,\mathrm{m}$ and $X = 89.9\,\mathrm{m}$.

2.2 Analytical model for wake vortex initialization

For this initialization method, we establish two fully rolled up counter-rotating wake vortices with a Lamb-Oseen profile of their tangential velocity. The wake vortices are separated by a distance of

$$b_0 = \frac{\pi}{4} b \tag{1}$$

with b denoting the span width. Their initial circulation is calculated with

$$\Gamma_0 = \frac{gM}{\rho_{air} b_0 U} \tag{2}$$

where g is the gravitational constant, M the mass of the aircraft, ρ_{air} the density of the air, and U the cruise speed. The initial descent speed of the imposed vortex pair is given by

$$w_0 = \frac{\Gamma_0}{2\pi b_0} \tag{3}$$

The mutual induction and the downward transport of the wake vortices are stronger for a larger circulation and smaller separation distance.

		A320	A380
Wing span	b/m	34.4	79.8
Circulation	$\Gamma_0/\mathrm{m}^2\mathrm{s}^{-1}$	240	720
core radius	r_c/m	3.0	4.5
Plume radius	R_{init}/m	12	25
Ice crystal number	$\mathscr{N}_0/10^{11}\mathrm{m}^{-1}$	8.52	46.07
Water vapor emission	$\mathscr{I}_0/(\mathrm{gm}^{-1})$	3.70	20.03
Mesh sizes (dx, dy/2, dz)/m		0.57	1.32
downstream positions of 2D slice:			
	X_1/m	4.3	10.0
	X_2/m	89.7	210.0

Table 1 – Aircraft-dependent parameters

2.3 LES model EULAG-LCM for contrail vortex phase simulations

The simulations of the early contrail evolution are carried out with the LES code EULAG-LCM. The base model EULAG [18] solves the Navier-Stokes momentum and energy equations in anelastic formulation. It employs the iterative upwind scheme MPDATA (Multidimensional Positive Definite Advection Transport Algorithm) [19] that has significantly less implicit diffusion compared to classical upwind schemes. The transport algorithm is at least second order and belongs to the non-oscillating forward-in-time schemes. EULAG is used for atmospheric applications from planetary to micro scales and a classical TKE turbulence model is used as subgrid model. The solution procedure with the underlying equation set is summarised in Section 2.1 of Unterstrasser [6].

A module for microphysics is fully coupled with EULAG resulting in the model version EULAG-LCM [20] that is able to simulate pure ice clouds like natural cirrus or contrails. It comprises explicit aerosol and ice microphysics with a Lagrangian ice particle tracking, homogeneous freezing of liquid supercooled aerosol particles, heterogeneous ice nucleation, deposition growth of ice crystals, sedimentation, aggregation, latent heat release, and radiative impact on particle growth. In the present study, it is not necessary to use all implemented microphysical processes. As in previous EULAG-LCM contrail vortex phase studies, deposition growth and latent heat release are the only processes switched-on. So-called simulation particles (SIPs) represent a certain number of (identical) real crystals and are advected by the fluid. Additionally, each SIP stores information, e.g. on the discrete position, the mass, and the habit of the bundled ice crystals. The transport equation is solved for each SIP by a Runge-Kutta scheme of second order. The particle velocity is a superposition of the fluid velocity (as obtained from the EULAG base model), an auto-correlated turbulent contribution, and lastly the terminal settling velocity in the vertical direction (since sedimentation is not relevant for the investigated case, this part is neglected). Not only the transport equation, but also the microphysical processes are computed for each SIP. So, the rate of change of the water vapour concentration can be derived by the summed up mass change of all SIPs in a grid box, which is a source term in the EULAG prognostic equation for water vapour concentration. Analogously, the latent heating is a source term for the temperature equation in EULAG. Furthermore, ice crystal concentrations can be derived from the SIP data in an a-posteriori step. Integrating this resulting 3D fields in some spatial directions, we obtain transverse and vertical profiles of, e.g., the total ice crystal number or mass per meter of flight path. Formulas associated to these definitions can be found in [6]. The vertical coordinate is defined such that the cruise altitude is at $z = 0$.

3. Simulation Setup

We simulate the contrails of A380 and A320 aircraft for two types of wake vortex initialization and analyse the effects on contrail geometrical and microphysical properties. The first step in this process is the creation of the RANS velocity fields that serve as input for EULAG-LCM. For that, both aircraft are modelled in 3D and the CFD simulations are performed with hybrid unstructured meshes. A detailed description how the TAU-MGLET simulation for the A320 is set up can be found in Stephan et al. [21]. Results of a similar TAU-MGLET simulation in high-lift configuration have already been

presented in Stephan et al. [22]. In more technical terms, a 2D plane (perpendicular to flight direction) is selected at a specific distance behind the aircraft from the CFD generated 3D velocity field and interpolated to a uniform Cartesian grid. This 2D slice serves as the initial velocity field for the temporal EULAG-LCM simulation, where the data is repeated in the third dimension. For a better comparison, the distances of the 2D slice downstream of the aircraft are measured from the tail of the aircraft and for both aircraft types the same normalized downstream positions are selected; $X_1 = 0.15b_0$ and $X_2 = 3.35b_0$ The absolute values can be found in Table 1. In the following, we will name this type of initialization as *RANSInit* or just label it with the distances specified in Table 1 for X_1 as *X04* (A320) and *X10* (A380) and for X_2 as *X90* (A320) and *X210* (A380).
For comparison with previous studies, further simulations are performed with an analytical wake vortex initialization as described above. In the following, we will refer to this initialization scenario as *anaInit*. For each aircraft, the parameters for the analytical wake vortex model are listed in Table 1. To compute the initial circulation values, the required values are taken from the Base of Aircraft Data (BADA) database [23]. Nearly all quantities listed in Table 1 scale with the wingspan. The A380 values are often larger than the A320 values by a factor of their wingspan ratio $b_{A380}/b_{A320} = 79.8/34.4$. In both initialisation scenarios, the contrail plumes are imposed as tubes with a specific radius R_{init} and spatially homogeneous ice crystal properties. We initialize the ice crystals such that their total mass is identical to the emitted mass of water vapour, which is given by

$$\mathscr{I}_0 = \frac{\dot{m}_f}{U} EI_{H20} \tag{4}$$

in terms mass per length of flight path. Similarly, the initial ice crystal number is computed with

$$\mathscr{N}_0 = \frac{\dot{m}_f}{U} EI_{iceno} \tag{5}$$

Here, $EI_{H20} = 1.25$ kg kg^{-1} is the water vapor emission index and EI_{iceno} the ice crystal emission index for which we assume an aircraft-independent value of $2.8 \cdot 10^{14}$ kg^{-1}. The fuel flow rates $\dot{m}_f$ at cruise speeds U are taken from BADA [23]. The corresponding $\mathscr{I}_0$ and $\mathscr{N}_0$ values are listed in Table 1. The atmospheric parameters are chosen as listed in Table 2 and have already been used, e.g. in Unterstrasser and Görsch [8]. We perform simulations with three different relative humidity values $RH_i^* = 100\%, 120\%$, and 140%, and two different atmospheric stability values, $\mathrm{N_{BV0}} = 1.15 \cdot 10^{-2}\mathrm{s}^{-1}$ and $\mathrm{N_{BV1}} = 0.5 \cdot 10^{-2}\mathrm{s}^{-1}$. Both initialization cases utilize the same background atmospheric turbulence.

Quantity	Value	Quantity	Value	Quantity	Value
T*	217K	p_0	250hPa	ρ_{air}	0.4kgm^{-3}
$\mathrm{N_{BV0}}$	$1.15 \cdot 10^{-2}\mathrm{s}^{-1}$	$\mathrm{N_{BV1}}$	$0.5 \cdot 10^{-2}\mathrm{s}^{-1}$	ε	$10^{-7}\mathrm{m}^s\mathrm{s}^{-3}$
nx	384-512	ny	200	nz	600-800

Table 2 – Aircraft-independent parameters

The grid sizes dx, dy, and dz are scaled with respect to the vortex separation b_0. The number of grid points in the flight direction (ny=200) is kept constant, resulting in a domain size of approximately $8b_0$, which allows the development of similar Crow instability modes [24]. Between $nz = 600$ and 856 grid points are used in the vertical direction and between $nx = 384$ and 512 grid points in the transverse direction, resulting in a sufficiently large domain to avoid interactions of the oscillating and descending vortices with the boundary. The larger domains are required for simulations with weaker stability and are therefore computationally more demanding. To obtain acceptable wall clock times, 320 CPUs were used in parallel to cope with the computational demands.

4. Results

The initial stage of the contrail life cycle is primarily influenced by the dynamics of trailing wake vortices, which induce both microphysical and geometrical transformations. These vortices descend, resulting in a substantial vertical expansion of the contrail. Notably, the adiabatic heating occurring inside these descending vortices can cause considerable ice crystal loss, as the relative humidity

decreases. The extent of the ice crystal loss depends, e.g., on ambient conditions such as relative humidity (RH_i^*) and temperature T [25]. Hence, we conducted 3D simulations of vortex phase across a range of relative humidity values $RH_i^* = 100\%, 120\%$, and 140%. Additionally, we vary the thermal stratification, as this significantly affects the wake vortex evolution and with it the spatial structure of the contrail plume. Given the crucial role of dynamics in this early stage, the initialization of the wake vortices may be of high importance for the early contrail evolution. Consequently, we investigate for the *RANSInit* simulations whether the downstream position X (see Table 1) of the wake vortex RANS data exerts an influence on the subsequent development of the contrail.

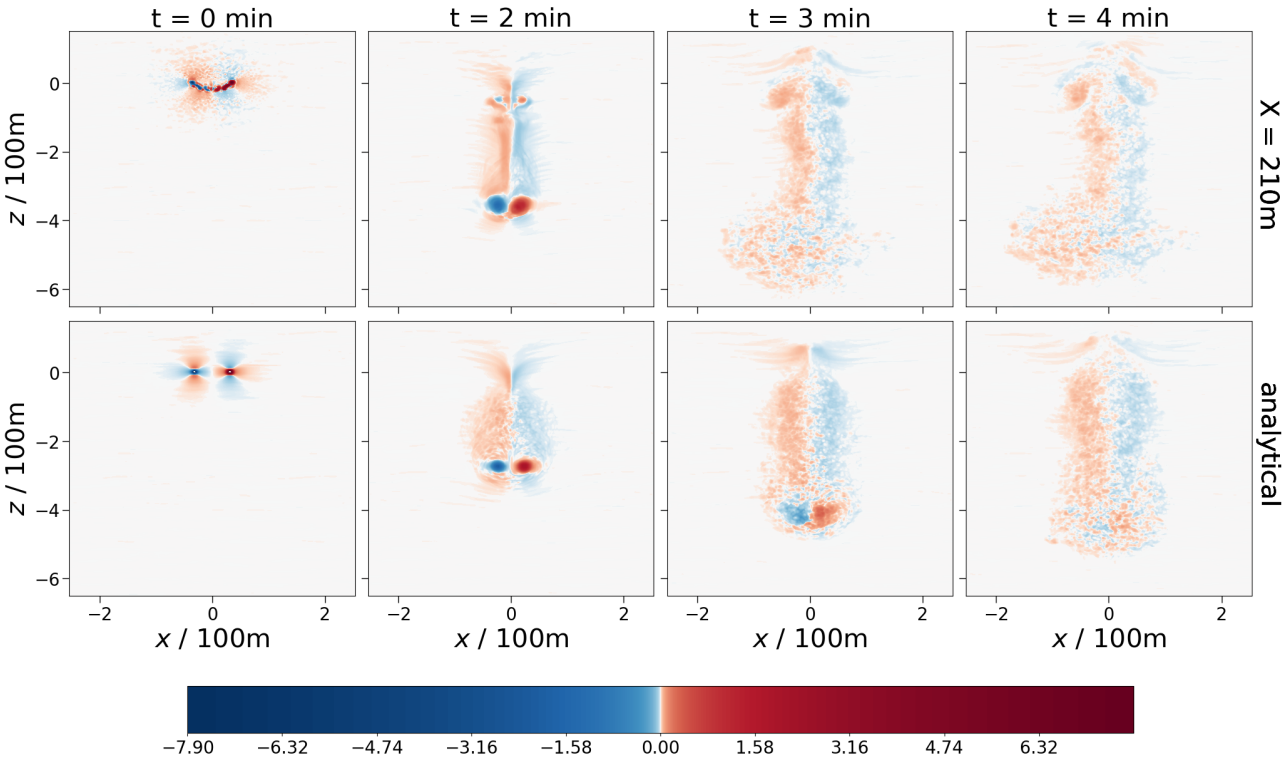

Figure 1 – Vorticity field of an A380 averaged in flight direction and at different simulation times $t \in \{0, 2, 3, 4\}\,\mathrm{min}$ for the RANS velocity field at $X = 210\,\mathrm{m}$ (top row) and of an analytical wake vortex profile initialization (bottom row).

4.1 Baseline Simulations

In this section, we present the evolution of the wake vortices and the contrail for an A380 and a A320 at a relative humidity of $RH_i^* = 120\%$. Fig. 1 illustrates the vorticity field of the A380 averaged in flight direction at different simulation times $t \in \{1, 2, 3, 4\}$ min (*RANSInit* for $X_2 = 3.35 b_0 = 210\,\mathrm{m}$, left; *analnit* right). It shows only the part of the domain where the wake vortices are visible, not the entire domain. Starting from an identical altitude at $z = 0\,\mathrm{m}$, after one minute the *RANSInit* wake vortex (top row) has descended further compared to its analytically initialised counterpart (bottom row). After three minutes, the former has already experienced a disruption of its core vortex structure, while the latter maintains its structural integrity for up to four minutes. This behaviour is probably due to the fact that the initial vortex separation in the RANS field is smaller than in the analytical setup, which uses Eq. 1. The smaller distance between the individual wake vortices in the *RANSInit* simulation leads to a faster descent of this pair and a stronger mutual interference, leading to an earlier structural breakdown.

The different descent rates are also apparent in the vertical profiles of the contrail ice mass, as depicted in Fig. 2 for several points in time. The dotted lines show the *RANSInit*-X_2 simulations, while the solid lines represent the *analnit* simulations. Cases for both aircraft are depicted: A380 (black) and A320 (red). A preliminary examination of the early contrail evolution of the A380 (black lines) reveals that while the total ice crystal mass remains similar with both initialization methods, there

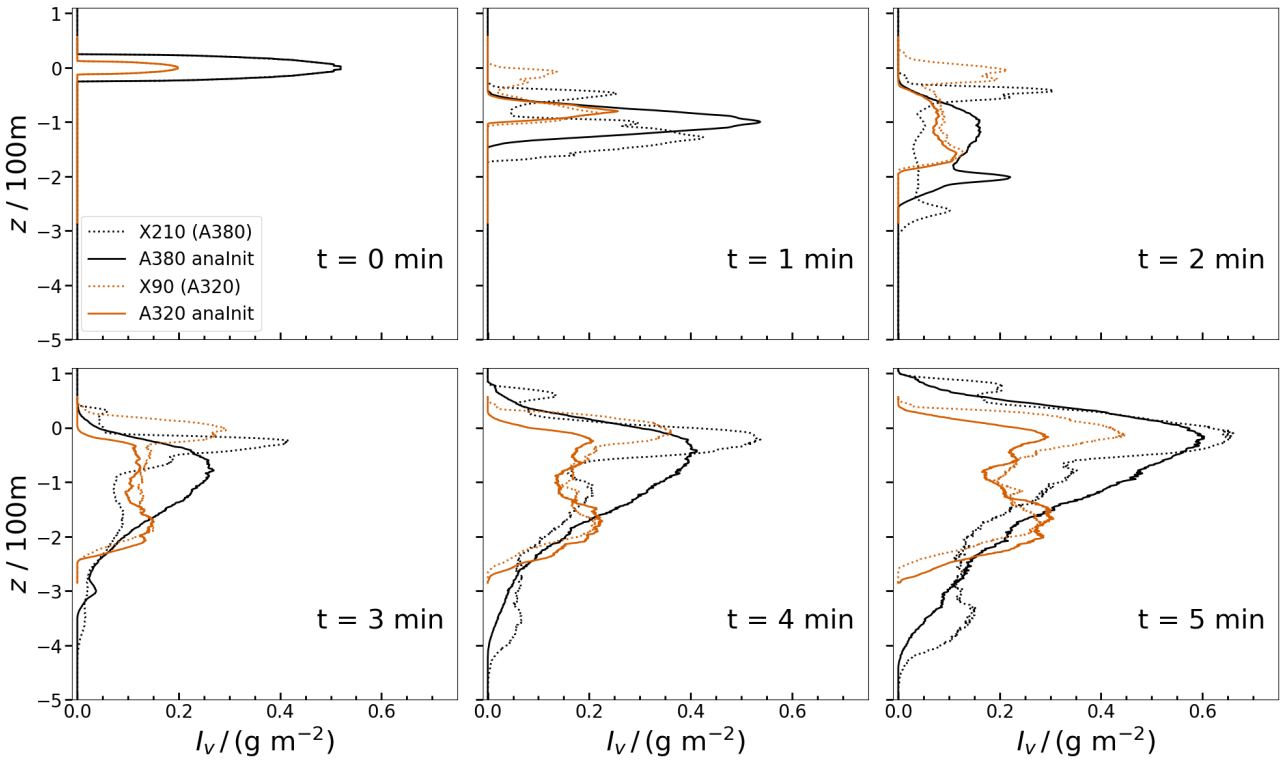

Figure 2 – The profile of the total ice crystal mass in vertical direction at different simulation times $t \in \{0, 1, 2, 3, 4, 5\}$ min at 120% ice saturation. The dotted line is the *RANSInit* and the solid line is the *analnit*, the black lines are for the A380 simulations and the red ones for the A320 simulations.

are discernible differences in their evolution and distribution. Despite the more rapid displacement of ice crystals in the beginning of the *RANSInit* simulation, the final vertical profile spans over the same altitude range of 550m. Additionally, the RANS-based profile appears more irregular. Previous simulations utilising an analytical wake vortex initialization exhibit that the majority of ice crystals are entrained within the wake vortex system during the roll-up process. In contrast, the RANS-based simulation features a more pronounced peak at the emission altitude, particularly at t=2 minutes. This is likely due to the fact that fewer ice crystals have been entrained into the wake vortex system, which then remain at the emission altitude.

A similar peak at the emission altitude can be found in the *RANSInit* simulation of the A320 hinting at a general pattern of fewer ice crystals being entrained for the RANS-based initialization. Unlike the A380 simulations, the A320 simulations do not shows a difference in the descent speed between two initialization types. After 5 minutes, the ice crystals in the *analnit* simulation have been transported to a slightly lower altitude than in the *RANSInit* simulation. A comparison of the A320 and A380 simulations reveals the dependency of the contrail vertical extent on the type of aircraft, as previously examined in Unterstrasser and Görsch [8].

In transverse direction, perpendicular to the flight direction, the two peaks of the initial ice crystal distribution of the *RANSInit* merge more rapidly than those of *analnit* for both aircraft (not shown). Nevertheless, the overall appearance and contrail width are similar.

4.2 Variation of Ambient Relative Humidity

As previously stated, the relative humidity level exerts a significant influence on the growth and sublimation of ice crystals. At $\mathrm{RH}_i^* = 100\%$, the number of ice crystals is almost zero in the end, while at $\mathrm{RH}_i^* = 140\%$, nearly all ice crystals survive the vortex phase. At $\mathrm{RH}_i^* = 120\%$, the impact of parameter changes on the extent of ice crystal loss is the largest [8]. Figure 4 shows the normalized ice crystal number $f_{\mathcal{N}}(t)$, which is the ice crystal number divided by its initial value. The plot depicts A380 simulations at three relative humidity values and for three initialization scenarios: the *analnit* simulation and the two *RANSInit* simulations, *X210* and *X10*.

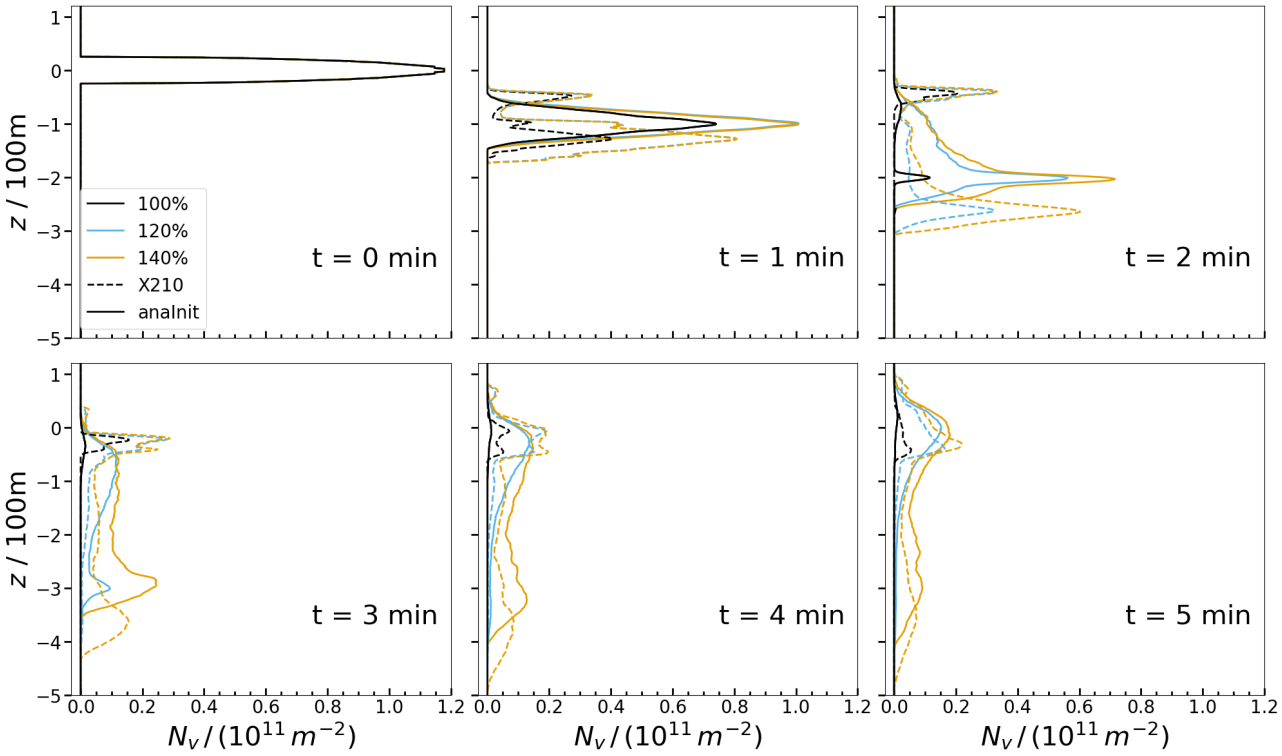

Figure 3 – The vertical profile of the total ice crystal number in z-direction at different simulation times $t \in \{0, 1, 2, 3, 4, 5\}\,\mathrm{min}$ and for $\mathrm{RH}_i^* = \{100\%, 120\%, 140\%\}$. The dotted lines represent the *RANSInit*, while the solid ones depict the *analnit*.

In very moist conditions, such as $\mathrm{RH}_i^* = 140\%$, ice crystals do not sublimate, but remain present until vortex break-up. This enables them to be regarded as passive tracers, thereby disclosing the wake dynamics. Hence, the final displacement of the wake vortices can be discerned from the vertical ice crystal distribution. As illustrated in Fig. 3, the ice crystals of the *RANSInit* (dotted yellow curve) have been transported down to a lower altitude compared to those of *analnit* (solid yellow curve). This discrepancy suggests that the wake vortices initiated through the *RANSInit* method descend at a faster rate and to a greater extent than their analytically initialized counterparts, resulting in a difference in height of nearly 100 meters. This difference is attributed to a smaller separation of the wake vortex pair in the 2D velocity field taken from the RANS simulation (see Section 4.4).

At a relative humidity of $\mathrm{RH}_i^* = 120\%$, the faster descent of the *RANSinit* vortices is also evident at the time $t = 2\,\mathrm{min}$ in Fig. 3. Subsequently, more ice crystals sublimate in the *RANSinit* contrail evolution, resulting in a diminished vertical extent. Due to the earlier breakup of wake vortices in this scenario, ice crystals are released into the surrounding atmosphere at an earlier point in time, where they dissipate at a faster rate. As anticipated, the number of sublimated ice crystals increases with lower humidity levels.

At low saturation levels, such as $\mathrm{RH}_i^* = 100\%$, a significant portion of the ice crystals undergo sublimation within the first three minutes; basically, all ice crystals that have been entrained in to the wake vortex system disappear. Only those ice crystals being not entrained may survive as they are not affected by adiabatic heating. Hence, the $\mathrm{RH}_i^* = 100\%$ can be used to analyse how the entrainment depends on the type of vortex initialisation. In comparison to the *analnit* scenario, where less than 5% of the initial ice crystal number persists, the survival rate of ice crystals for the two *RANSInit* scenarios is approximately twice as large. The wake vortex pair in the latter scenario is not fully rolled up, which explains why some ice crystals are not captured within the wake but remain at the aircraft's flight altitude.

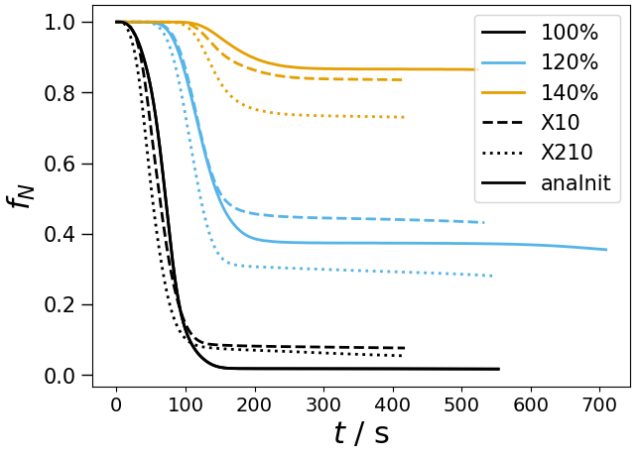

Figure 4 – The evolution in time of the normalized ice crystal number is displayed for different relative humidity $\mathrm{RH}_i^* = \{100\%, 120\%, 140\%\}$ and a Brunt-Väisälä frequency of $\mathrm{N}_{BV0} = 1.15 \cdot 10^{-2}\mathrm{s}^{-1}$. The dashed and dotted lines represent the initialization method with the RANS flow field, while the solid ones depict the analytical wake vortex profile initialization.

4.3 Weak Thermal Stability

In this section, we present simulations with weaker thermal stability. In this scenario, wake vortices tend to descend further and exhibit stronger meandering. This necessitates, e.g. also an increase in the simulation domain to $nx = 512$ and $nz = 800$ grid points.

We examined the differences between the two initialization methods (*analnit* and *RANSInit*) for the A380 in an atmosphere with weaker thermal stability, characterized by $N_{BV1} = 0.5 \cdot 10^{-2}\mathrm{s}^{-1}$ and a relative humidity of $RH_i^* = 140\%$.

As previously discussed, the wake vortices descend more rapidly with *RANSInit* compared to *analnit*. For weaker stratification, again the wake vortices with *RANSInit* descend more quickly, but only up to $t = 2$ minutes (Figure 5, blue dotted line represents *RANSInit* and the blue solid line represents *analnit*). Once they reach an altitude 400 meters below the emission altitude, the sublimation process becomes dominant, causing the lower boundary to rise by approximately 50 meters. A significant portion of ice crystals is not entrained in the wake vortex and initially remains at the emission altitude before rising up to 100 meters above this altitude, as observed in the *RANSInit* simulation within a stably stratified atmosphere (yellow dotted line). The ice crystals initialized with *analnit* descend further than those with *RANSInit*, reaching nearly 600 meters below the emission altitude, with none rising back to the flight level.

According to Unterstrasser and Görsch [8], the vertical extent of the ice crystal profile in an *analnit*

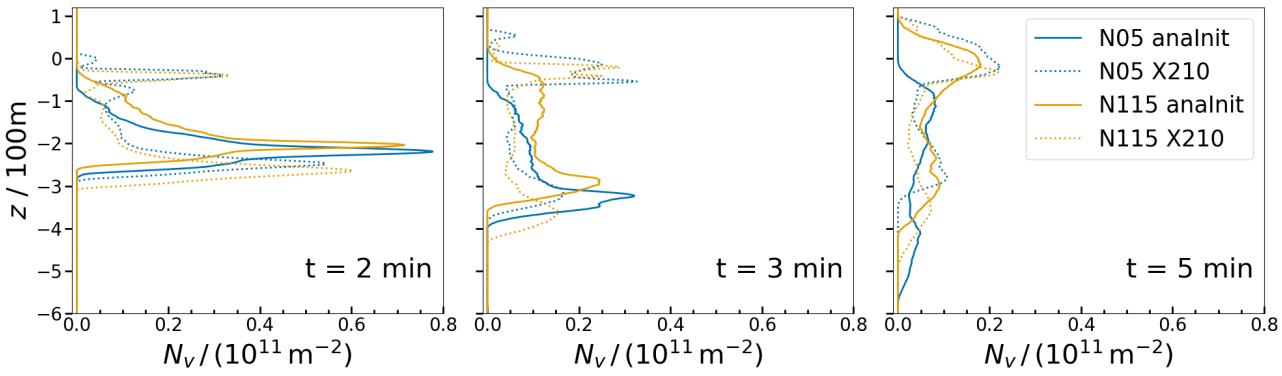

Figure 5 – The vertical profiles of ice crystal numbers (spanwise integrated and averaged along flight direction) at $t = \{2, 3, 5\}$ min in a weaker stratified atmosphere ($\mathrm{N}_{BV1} = 0.5 \cdot 10^{-2}\mathrm{s}^{-1}$, blue curves) and in the stronger stratified atmosphere ($\mathrm{N}_{BV0} = 1.15 \cdot 10^{-2}\mathrm{s}^{-1}$, yellow curves) at $\mathrm{RH}_i^* = 140\%$ for the*X210* (dotted curves) and the *analnit* (solid curves).

simulation increases under weaker thermal stratification. However, the opposite trend is observed for the *RANSInit* method. In the current study, the vertical extent of the profile with N_{BV1} is approximately 425 meters, compared to nearly 600 meters for N_{BV0} (stable stratification). The number of surviving ice crystals is significantly higher for the *RANSInit* method than for the *analnit* method under weak stratification, whereas the reverse is true in the stable stratification scenario.

4.4 Impact of Downstream Position

As previously discussed, the dynamics significantly influence the evolution of the contrail. Therefore, the precise downstream position where the 2D velocity field is extracted is crucial. In order to investigate this phenomenon, we examine the evolution of contrails for both aircraft (A320 and A380) at two different initialization positions: $X_1 = 0.15b_0$ and $X_2 = 3.35b_0$. The exact values for both aircraft types are provided in Table 1. At both positions, the wake vortices are not yet fully developed. However, at X_2, the wakes are at a slightly more advanced stage of development compared to X_1, indicating a greater degree of vortex roll-up. The results for the A380 are presented first, followed by those for the A320.

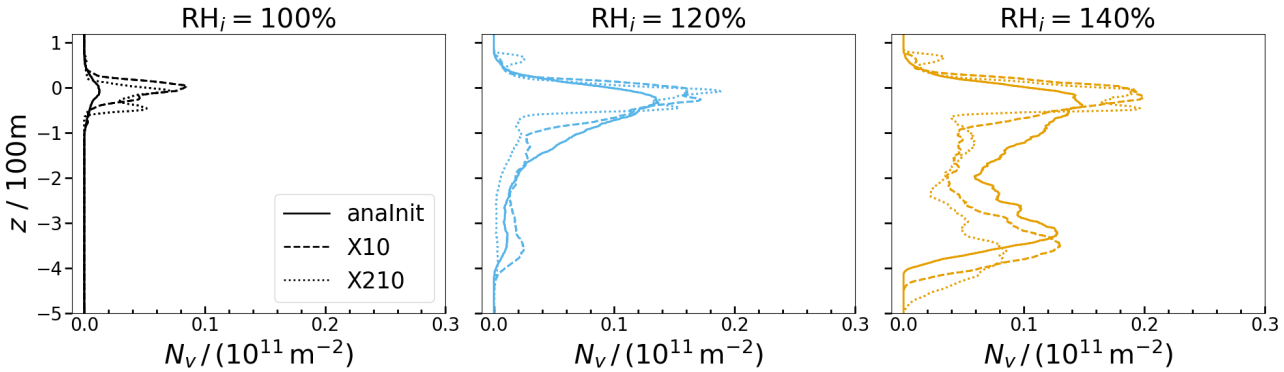

Figure 6 – The vertical profile of the total ice crystal number behind an A380 after 4min for different relative humidity: $\mathrm{RH}_i^* = 100\%$ (left), $\mathrm{RH}_i^* = 120\%$ (middle), and $\mathrm{RH}_i^* = 140\%$ (right).

In Fig. 6, the vertical profile of the ice crystal number is shown for the A380 and three different relative humiditiy values ($\mathrm{RH}_i^* = 100\%$, $\mathrm{RH}_i^* = 120\%$, and $\mathrm{RH}_i^* = 140\%$) after four minutes. On the right side, at a relative humidity of 140%, the influence of different dynamical initializations becomes apparent, as only a minimal number of ice crystals sublimate over time. For the initialization with the 2D RANS flow field slice at $X_2 = 210\,\mathrm{m}$ (*X210*), the ice crystals descend further compared to the $X_1 = 10\,\mathrm{m}$ (*X10*) case and the *analnit* case. This results in a vertical extent of almost 600 meters for *X210*, approximately 550 meters for *X10*, and 450 meters for *analnit*. Due to the increase in temperature with decreasing altitude, most ice crystals sublimate in the *X210* scenario (Figure 4). The pronounced ice crystal peak at the emission altitude is comparable between the two *RANSInit* cases. At a relative humidity of $\mathrm{RH}_i^* = 120\%$, the ice crystals loss is strongest in the *X210* case; yet, more crystal survive now in the *X10* case than in the *analnit* case. Although the vertical extent remains consistent for the latter, it reduces slightly (by approximately 10 meters) for the *X10* case and significantly (by approximately 250 meters) for *X210*. The ice crystal peaks at the emission altitude are also comparable between the *RANSInit* cases but more pronounced than in the *analnit* case. At a relative humidity of 100%, only $2-10\%$ of ice crystals survive. In this scenario, the *analnit* method experiences the most ice loss, while the loss for *X10* and *X210* is similar, with the ice crystals in the latter case descending slightly further. The overall depth of the contrail is approximately 100 meters for all three scenarios.

Contrary to the A380 simulation results, the most significant ice crystal loss at a relative humidity of $\mathrm{RH}_i^* = 120\%$ occurs for the **A320** with the *analnit* initialization (Figure 7). The ice crystal loss observed when initialized with the 2D RANS flow field taken at a distance of $X_1 = 4,3\,\mathrm{m}$ (*X04*) is smaller compared to when initialized with the flow field taken at a distance of $X_2 = 80.79\,\mathrm{m}$ (*X90*).
In Figure 8, the vertical ice crystal profile is depicted for $t \in \{2,3,5\}$ minutes. The ice crystals from the *analnit* method (red solid line) descend slightly faster than those from *X90* (blue dotted). Notably,

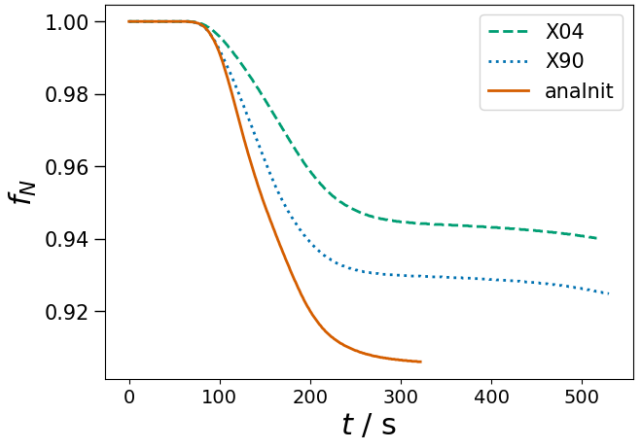

Figure 7 – The evolution in time of the normalized ice crystal number behind a A320 is displayed for a relative humidity $\mathrm{RH}_i^* = 120\%$ and a Brunt-Väisälä frequency of $\mathrm{N}_{BV0} = 1.15 \cdot 10^{-2}\mathrm{s}^{-1}$. The dashed and dotted lines represent the initialization method with the RANS flow field, while the solid ones depict the analytical wake vortex profile initialization.

following the vortex breakup at $t = 4$ minutes, the ice crystals from *analnit* are transported further downward. Conversely, the ice crystals from *X04* (green dashed) descend more slowly than those from *X90*, particularly after $t = 2$ minutes, and also more slowly than those from *analnit*. Moreover, the downward transport of ice crystals from *X04* halts at a higher altitude (approximately 50 m) after $t = 4$ minutes compared to *X90*.
In accordance with the A380 simulation, an ice crystal peak forms at flight altitude for both *RANSInit* cases but not for *analnit*. The final vertical extent after vortex breakup is nearly 300 m for *analnit*, 250 m for *X90*, and 200 m for *X04*.

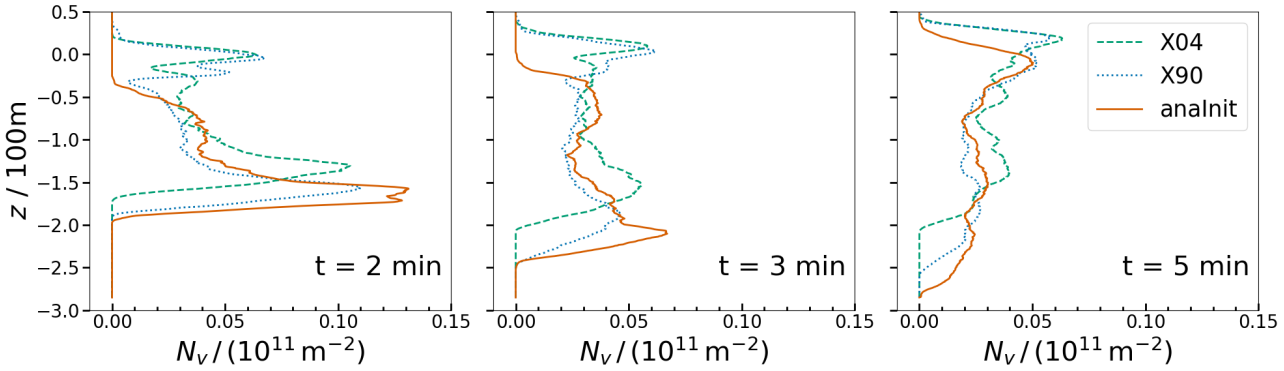

Figure 8 – The vertical profile of the total ice crystal number of a A320 with the *RANSInit* at a downstream position of 4m (*X04*, green dashed) and 90m (*X90*, blue dotted) as well as the *analnit* (red solid) after $t = \{2, 3, 5\}$ min for $\mathrm{RH}_i^* = 120\%$.

The differing vertical descent speeds of *analnit* and *RANSInit* can be attributed to the variations in the distances between the wake vortex centers and the circulation values (Figure 9). For the **A380** simulation, the circulation of *analnit* is lower during the first 120 seconds compared to *RANSInit* (Figure 9a). Additionally, the wake vortex separation is significantly greater for *analnit*. These factors result in a smaller induced downforce between the wake vortices, leading to a reduced downward velocity and a reduction in the descent altitude compared to the wake vortices in the two *RANSInit* cases, as previously described.
When comparing the two A380 *RANSInit* scenarios, it is observed that the circulation in the *X210* case is marginally higher than in *X10*, and the distance from the wake vortex center is slightly smaller for most of the time. This minor difference in parameters results in a slightly higher descent rate for

the wake vortices in the *X210* scenario, causing them to travel further downward within the same timeframe compared to those in the *X10* scenario.
The vorticity evolution depicted in Figure 1 clearly illustrates the slower descent velocity of *analnit*, particularly at $t = 2$ minutes. The difference in final altitude at $t = 4$ minutes is evident when comparing *analnit* with *X210*, where the lowest altitude was already reached at $t = 3$ minutes.
In light of these findings, another *analnit* simulation for the A380 was conducted with adjusted circulation and wake vortex distance values (*analnitComp*), which aligned more closely with the expected parameters (green dash-dotted line in Figures 9a and 9b). The vertical profile for this adapted simulation is presented in the subsequent section.

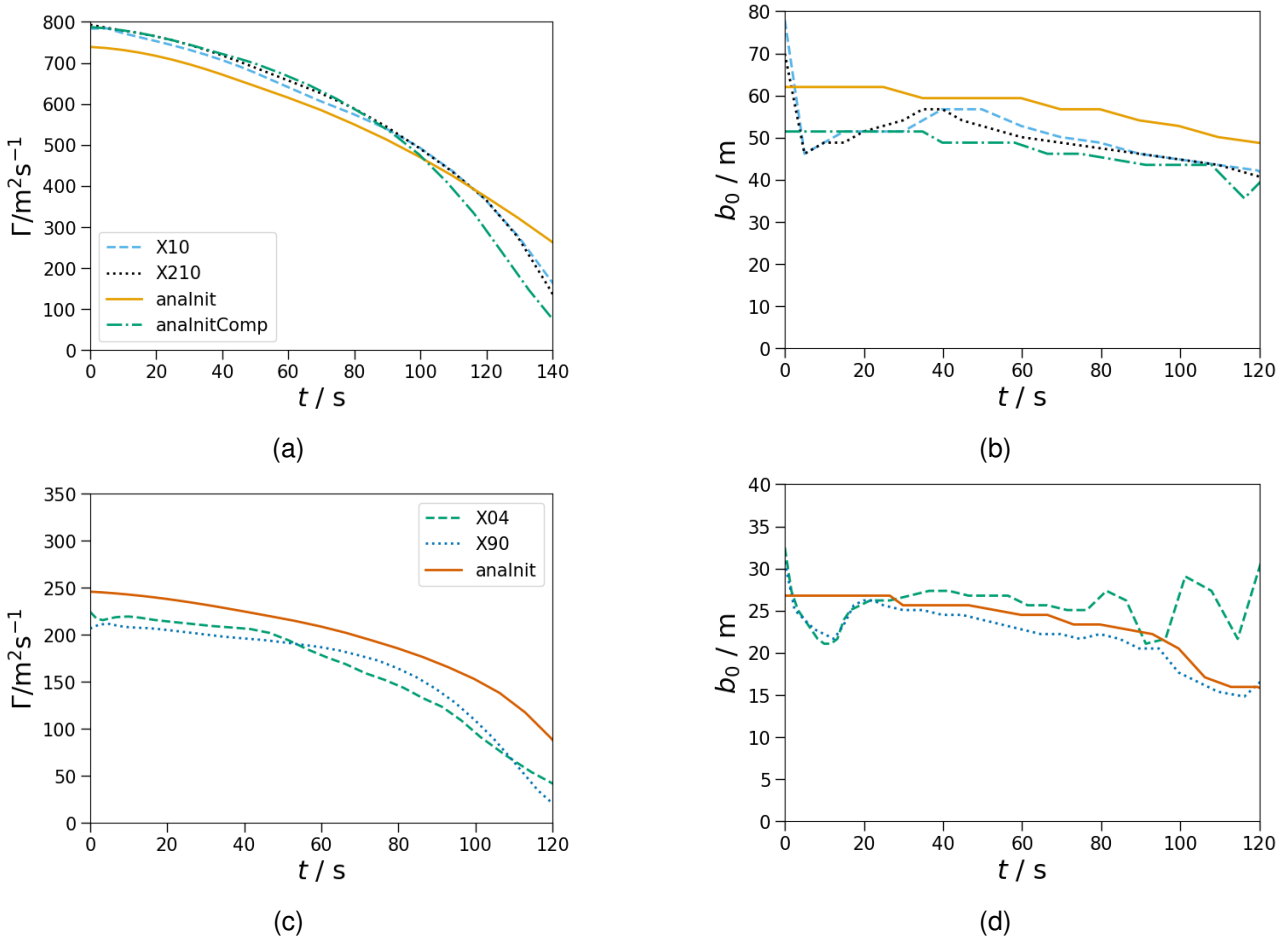

Figure 9 – The temporal evolution of the (a) circulation and (b) the vortex distance of four different A380 initialization scenarios: *X10*(light blue dashed) and *X210* (black dotted), an analytical initialization with aircraft parameters as stated in Table 1 (*analnit*, yellow solid) and adapted parameters ($\Gamma = 770$ m^2/s^{-1}, $b_0 = 52.2$ m,*analnitComp*, green dash-dotted). And the temporal evolution of (c) circulation and (d) the wake vortex distance of an A320 with *analnit* (red solid), *X04* (green dasehd), and *X90* (blue dotted).

For the **A320**, the circulation of the *analnit* overestimates the circulation of the two *RANSInit* simulations (Fig. 9c), whereas the distance of the wake vortex center is estimated quite well (Fig. 9d). Especially after 20s, it follows the vortex center distance of *X90* quite well. In the first 20s, the *RANSInit*s' wake vortex distance has a dip, which was also already visible for the A380. This effect is either due to the still ongoing roll-up process of the wakes or because of our method for detecting the wake vortex center. After approximately 80 seconds, the determination of the wake vortex center for *X04* is not reliably anymore with our detection method and the distance value in the graph starts to oscillate.
For the **A320** simulations, the circulation of the *analnit* overestimates the circulation observed in the two *RANSInit* simulations (Figure 9c). However, the distance of the wake vortex center is accurately

estimated (Figure 9d). Particularly after 20 seconds, it closely follows the vortex center distance of the *X90* simulation. In the first 20 seconds, the *RANSInit* wake vortex distances exhibit a dip, a phenomenon also observed for the A380. This dip may result from the ongoing roll-up process of the wakes or from our method of detecting the wake vortex center. After approximately 80 seconds, accurately determining the wake vortex center for *X04* becomes increasingly difficult using our detection method, leading to oscillations in the distance values on the graph.

4.5 Comparable Aircraft Parameter Simulation

In the previous section, differences were identified in the aircraft-dependent parameters between the *RANSInit* and *anaInit* simulations, specifically the distance between the wake vortex centers and the amount of circulation. Consequently, a second *anaInit* simulation was conducted with $\Gamma = 770\,\mathrm{m}^2/\mathrm{s}$ and a wake vortex distance of $b_0 = 52.2\,\mathrm{m}$ at a relative humidity of $RH_i^* = 140\%$. This simulation is referred to as *anaInitComp*. Figures 9a and 9b demonstrate that, with these adjusted values, the wake vortex parameters are closer to those of the *RANSInit* simulation.

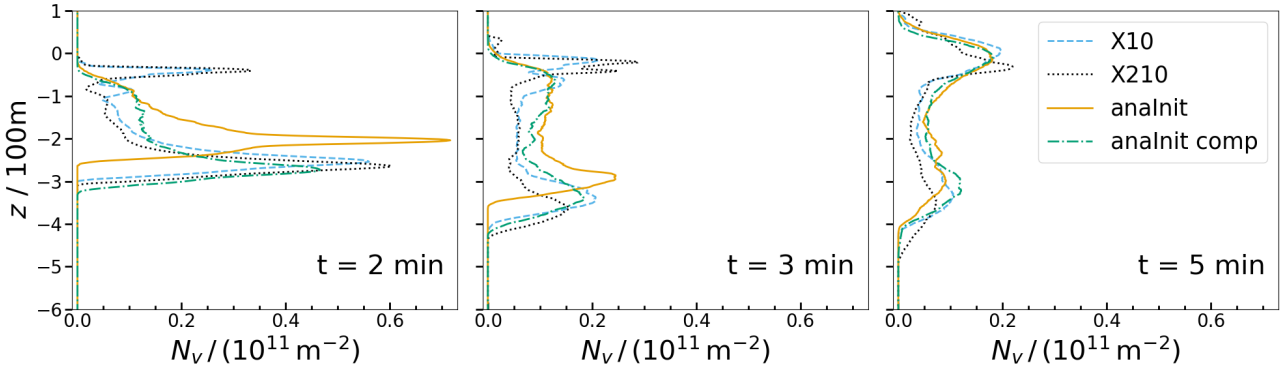

Figure 10 – The profile of the total ice crystal number in vertical direction after $t = \{2, 3, 5\}$ min for a relative humidity of $\mathrm{RH}_i^* = 140\%$ for 4 different initialization: the two *RANSInit X10* (light blue dashed) and *X210* (black dotted), and the two *anaInit* (yellow solid) and *anaInitComp* (green dash-dotted).

The temporal evolution of the total number of ice crystals and the amount of ice mass does not significantly differ from the original *anaInit* simulation. In the transverse direction, the ice crystal distribution of *anaInitComp* closely matches that of *anaInit* for most of the simulation period.
Vertically (Fig. 10), the ice crystals in the *anaInitComp* simulation (green dash-dotted line) descend with the same velocity as in the *RANSInit* simulations (light blue dashed and black dotted line). After 5 minutes, the descent of the ice crystals halts at the same altitude as observed in the *anaInit* and *X10* simulations. However, the previously described peak of ice crystals at the emission altitude in the *RANSInit* simulations does not occur in the *anaInitComp* simulation.

5. Discussion

In this study, we focused on the impact of the initialization method on the evolving contrail. The *anaInit* was employed in former simulation investigations [8, 10, 12, 13]. The more realistic *RANSInit* reveals new insights: not all ice crystals are entrained in the downwards moving wake vortex system but stay at the emission altitude. This effect matches with observations during flight campaigns [13].
The values used for wake vortex distance and circulation in the *anaInit* and in [8, 10] method do not necessarily agree with the values of the RANS simulation of the full aircraft geometry leading to differences in the contrail evolution. The vertical extent of the *RANSInit* contrails varies with the utilized downstream position and is either smaller or bigger than the one of *anaInit* that agree well with Unterstrasser and Görsch [8]. The differences in the early contrail evolution of different aircraft types elaborated in Unterstrasser and Görsch [8] could be confirmed with our study.
Our process to simulate the contrail evolution is already on a high standard, nevertheless we want to compare it to the methods used in Saulgeot et al. [26].

6. Conclusion

In this study, we employ the large eddy simulation model EULAG-LCM, incorporating a Lagrangian microphysics module, to simulate the evolution of contrails over the first five minutes using various initialization methods. The simulation results of the initialization with an analytical wake vortex profile are compared to those initialized with a RANS flow field around a fully modeled aircraft. This comparison covers two different aircraft types (A320 and A380). Moreover, we varied the background relative humidity, as this has a significant impact on contrail microphysics and the thermal stratification, which in turn affects wake vortex displacement and lifetime. Our findings reveal that with the RANS initialization method, not all ice crystals are captured within the wake vortices and are carried downward with the descending wake; a significant portion remains at the emission altitude. The vertical distribution of the ice crystals is highly dependent on the wake vortex dynamics. The results of the simulation with the RANS initialization exhibited an overestimation or underestimation of the vertical extent observed in the simulation with an analytically initialized wake profile, contingent on the degree of agreement between the wake distances and circulation values in both initialisation methods. An analytically initialized simulation with adjusted circulation and wake vortex distance value could replicate the dynamic behavior and vertical distribution of the ice crystals but could not reproduce the emerging peak at the flight altitude. Additionally, the exact downstream position of the 2D flow field slice for the RANS initialization method significantly influences early contrail evolution and requires further investigation. The results of this study demonstrate that the RANS initialization method significantly influences the early stages of contrail evolution behind a single aircraft. This finding suggests that this refined initialization method also has a substantial impact on contrail evolution in a formation flying scenario.

Acknowledgement

This work contributes to the EU project GEESE ("Gain Environmental Efficiency by Saving Energy", https://doi.org/10.3030/101114611). This work used resources of the Deutsches Klimarechenzentrum (DKRZ) granted by its Scientific Steering Committee (WLA) under project ID bd0832. Special thanks to Airbus and Simon Trapier for providing the RANS flow field data of the A380. The authors gratefully acknowledge the Gauss Centre for Supercomputing e.V. (www.gauss-centre.eu) for funding this project by providing computing time on the GCS Supercomputer SuperMUC-NG at Leibniz Supercomputing Centre (www.lrz.de) under project ID pn98me.

Copyright Statement

References

[1] D. S. Lee, D. W. Fahey, A. Skowron, M. R. Allen, U. Burkhardt, Q. Chen, S. J. Doherty, S. Freeman, P. M. Forster, J. Fuglestvedt, A. Gettelman, R. R. De León, L. L. Lim, M. T. Lund, R. J. Millar, B. Owen, J. E. Penner, G. Pitari, M. J. Prather, R. Sausen, and L. J. Wilcox. The contribution of global aviation to anthropogenic climate forcing for 2000 to 2018. *Atmos. Environ.*, 244:117834, 2021.

[2] U. Burkhardt and B. Kärcher. Global radiative forcing from contrail cirrus. *Nature Clim. Ch.*, 1(1):54–58, 2011.

[3] B. Kärcher and F. Yu. Role of aircraft soot emissions in contrail formation. *Geophys. Res. Lett.*, 36:L01804, 2009.

[4] A. Bier, S. Unterstrasser, and X. Vancassel. Box model trajectory studies of contrail formation using a particle-based cloud microphysics scheme. *Atmos. Chem. Phys.*, 22(2):823–845, 2022.

[5] A. Bier, S. Unterstrasser, J. Zink, D. Hillenbrand, T. Jurkat-Witschas, and A. Lottermoser. Contrail formation on ambient aerosol particles for aircraft with hydrogen combustion: a box model trajectory study. *Atmos. Chem. Phys.*, 24(4):2319–2344, 2024.

[6] S. Unterstrasser. Large eddy simulation study of contrail microphysics and geometry during the vortex phase and consequences on contrail-to-cirrus transition. *J. Geophys. Res.*, 119(12):7537–7555, 2014.

[7] D. C. Lewellen, O. Meza, and W. W. Huebsch. Persistent contrails and contrail cirrus. Part 1: Large-eddy simulations from inception to demise. *J. Atmos. Sci.*, 71(12):4399–4419, 2014.

[8] S. Unterstrasser and N. Görsch. Aircraft-type dependency of contrail evolution. *J. Geophys. Res.*, 119(24):14,015–14,027, 2014.

[9] Robert Sausen, Sina Hofer, Klaus Gierens, Luca Bugliaro, Rüdiger Ehrmanntraut, Ilona Sitova, Kacper Walczak, Anja Burridge?Diesing, Milena Bowman, and Nick Miller. Can we successfully avoid persistent contrails by small altitude adjustments of flights in the real world? *Meteorol. Z.*, 2023.

[10] S. Unterstrasser and A. Stephan. Far field wake vortex evolution of two aircraft formation flight and implications on young contrails. *Aeronaut. J.*, 124:667–702, 2020.

[11] Simon Unterstrasser. The Contrail Mitigation Potential of Aircraft Formation Flight Derived from High-Resolution Simulations. *Aerospace*, 7(12):170, 2020.

[12] R. Paoli, L. Nybelen, J. Picot, and D. Cariolle. Effects of jet/vortex interaction on contrail formation in supersaturated conditions. *Phys. Fluids*, 25(053305):1–28, 2013.

[13] P. Jeßberger, C. Voigt, U. Schumann, I. Sölch, H. Schlager, S. Kaufmann, A. Petzold, D. Schäuble, and J.-F. Gayet. Aircraft type influence on contrail properties. *Atmos. Chem. Phys.*, 13(23):11965–11984, 2013.

[14] Dieter Schwamborn, Thomas Gerhold, and Ralf Heinrich. The dlr tau-code: Recent applications in research and industry. 2006.

[15] M. Manhart. A Zonal Grid Algorithm for DNS of Turbulent Boundary Layers. *Comput. Fluids*, 33(3):435–461, 2004.

[16] Anton Stephan, Stefan Zholtovski, and Frank Holzapfel. Formation flight and wake vortex encounters with fully coupled hybrid rans/les. In *55th 3AF International Conference on Applied Aerodynamics FP44-AERO2020-stephan 23 25 March 2020, Poitiers France*, 2020.

[17] Frank Spiering. Coupling of tau and trace for parallel accurate flow simulations. In *Third Symposium "Simulation of Wing and Nacelle Stall"*, June 2012.

[18] J.M. Prusa, P.K. Smolarkiewicz, and A.A. Wyszogrodzki. EULAG, a computational model for multiscale flows. *Comput. Fluids*, 37(9):1193–1207, 2008.

[19] P.K. Smolarkiewicz and L.G. Margolin. MPDATA: A Finite-Difference Solver for Geophysical Flows. *J. Comput. Phys.*, 140(2):459–480, 1998.

[20] I. Sölch and B. Kärcher. A large-eddy model for cirrus clouds with explicit aerosol and ice microphysics and Lagrangian ice particle tracking. *Q. J. R. Meteorol. Soc.*, 136:2074–2093, 2010.

[21] Anton Stephan, David Rohlmann, Frank Holzäpfel, and Ralf Rudnik. Hybrid numerical simulation of the jet-wake-vortex interaction of a cruising aircraft. 2018.

[22] A. Stephan, D. Rohlmann, F. Holzäpfel, and R. Rudnik. Effects of Detailed Aircraft Geometry on Wake Vortex Dynamics During Landing. *J. Aircraft*, 56(3):974–989, 2019.

[23] Angela Nuic. User manual for the Base of Aircraft Data (BADA), Revision 3.9. Technical report, EEC Technical/Scientific Report No. 11/03/08-08, EUROCONTROL, 2011.

[24] S.C. Crow. Stability theory for a pair of trailing vortices. *AIAA Journal*, 8:2172–2179, 1970.

[25] S. Unterstrasser. Properties of young contrails - a parametrisation based on large-eddy simulations. *Atmos. Chem. Phys.*, 16(4):2059–2082, 2016.

[26] Pierre Saulgeot, Vincent Brion, Nicolas Bonne, Emmanuel Dormy, and Laurent Jacquin. Effects of atmospheric stratification and jet position on the properties of early aircraft contrails. *Phys. Rev. Fluids*, 8:114702, 2023.